A Low-Phase-Noise Multi-Phase Oscillator Based on Left-Handed LC-Ring

Guansheng Li and Ehsan Afshari, *Member, IEEE*

Abstract—This paper presents a distributed multi-phase oscillator based on left-handed LC-ring. In contrast to traditional designs that couple multiple LC-tanks through MOSFETs, it uses an LC-ring as a single high-order resonator that generates multi-phase resonant signal. By avoiding coupling MOSFETs which deteriorate phase noise significantly, it can synthesize multiple phases while maintaining the same phase-noise figure-of-merit (FoM) as a single-stage LC oscillator. This also provides a systematic way of trading power for phase noise. The dynamics and the phase noise of the LC-ring oscillator are analyzed based on a mode-decomposition model. We also address the duality of left-/right-handed resonator in the context of oscillator in detail. These analysis was verified by prototypes in a 0.13 μm CMOS process with 0.5 V supply voltage: a four-stage LC-ring oscillator at 5.12 GHz draws 8 mA current and achieves a phase noise of -121.6 dBc/Hz@600 kHz, while a single-stage one at 5.34 GHz draws 2 mA and achieves -116.1 dBc/Hz@600 kHz. There is a good agreement among analysis, simulation, and measurement.

Index Terms—LC-ring, left-handed structure, low phase noise, multi-phase oscillator, quadrature oscillator.
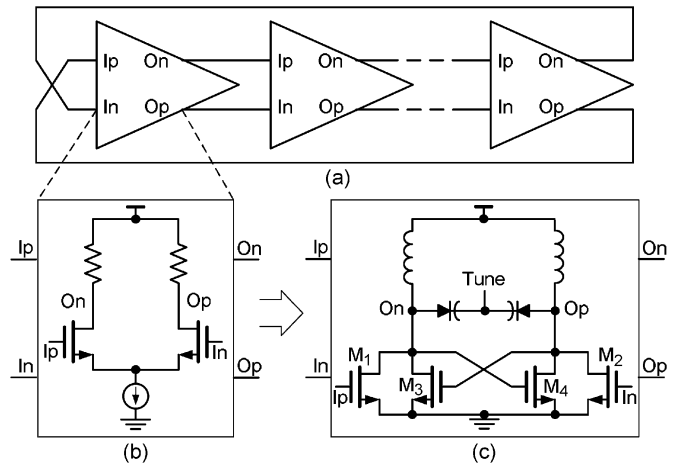
Fig. 1. Illustration of traditional ring oscillator: (a) general structure, (b) purely active gain stage, and (c) LC-boosted gain stages. The cross-coupled quadrature oscillator [8] can be recognized as a two-stage LC-boosted ring.

I. INTRODUCTION

MULTI-PHASE and quadrature oscillators are essential parts of many electronic systems, such as image rejection demodulator in wireless transceivers [1], half-rate clock-data-recovery (CDR) circuitry in high-speed optical receivers [2], [3], phased arrays [4], direct-conversion transmitters [5] and fractional-N frequency synthesizers [6]. As a result, there has been great interest in the design of low-phase-noise, low-phase-error multi-phase and quadrature oscillators.

Ring oscillator is inherently multi-phase, and an even-number-stage differential ring (Fig. 1(b)) can generate quadrature signals. However, it suffers from high phase noise [7]. LC-boosted ring oscillator incorporates high-quality *LC* tanks to lower phase noise (Fig. 1(c)). This structure includes the widely-used cross-coupled quadrature *LC* oscillator [8], which is a two-stage ring. However, the phase noise performance of LC-boosted ring oscillator is still inferior to single-stage *LC* oscillator, largely due to the trade-off between phase noise and phase error. On the one hand, small phase error requires strong

coupling between the gain stages, which prefers large coupling MOSFETs, i.e., M_1 and M_2 in Fig. 1(c); on the other hand, large coupling MOSFETs penalize phase noise and increase power consumption. In particular, in a two-stage ring, the drain current and drain voltage of the coupling MOSFETs are in quadrature, which means they only resonate with the *LC* tanks and do not deliver net energy. Moreover, this resonance with MOSFETs introduces extra noise to the *LC* resonator, as the channel current of MOSFETs is typically much noisier than the resonant current in inductors and capacitors. A few other *LC* quadrature oscillators have also been proposed, such as the super-harmonic-coupled structure [1], but their phase noise performance still needs improving. In general, there is typically a 5 dB to 10 dB gap in phase-noise figure-of-merit (FoM) between reported multi-phase/quadrature *LC* oscillators [10]–[13] and single-stage *LC* oscillators [14], [15], where the FoM is defined as

$$\text{FoM} = 20\log\left(\frac{f_0}{\Delta f}\right) - L(\Delta f) - 10\log P_{\text{diss}|\text{mW}} \quad (1)$$

with f_o, Δf, $L(\Delta f)$ and $P_{diss|mW}$ denoting the oscillation frequency, the offset frequency, the phase noise in dBc/Hz and the power consumption in mW, respectively.

In all these multi-phase/quadrature *LC* oscillators, MOSFETs play a dual role: 1) compensate the energy loss in *LC* tanks; 2) couple *LC* tanks together and maintain a desired phase relation. But, as discussed above, the second task usually deteriorates phase noise, and, in particular, causes significant flicker noise

Fig. 2. Illustration of left-handed mobius-connected LC-ring oscillator.
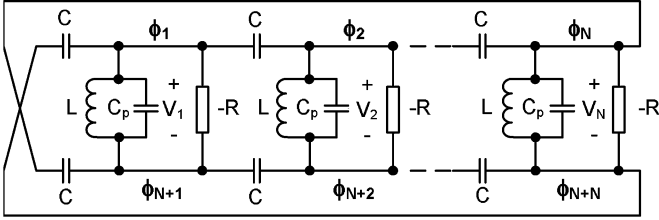

Fig. 3. Illustration of single-ended LC-ring structure.

up-conversion [16]. This encourages us to shift it from MOS-FETs to passive devices, by using a single high-order LC resonator generating multi-phase signals.

In this paper, we present a distributed oscillator based on left-handed [17], [18] LC-ring, as illustrated in Fig. 2, which consists of identical LC stages with series capacitance and shunt inductance. The LC-ring is a single resonator that generates multi-phase resonant signals. The MOSFETs only need to compensate the energy loss of the LC-ring as negative resistors, i.e., the current from active devices is always injected into the resonator in phase with voltage and does not resonate with passive devices. Analysis shows, for an N-stage LC-ring oscillator, the phase noise scales down as $1/N$, while the power consumption increases linearly with N. Thus, one can synthesize multiple phases while maintaining the same phase-noise FoM as a single-stage LC oscillator. This also provides a systematic way of trading power for phase noise, which can be used to meet the stringent phase noise requirement in low-supply-voltage applications [16].

Distributed oscillators based on transmission lines [19], [20] or lumped elements [21] were extensively studied. However, the resonators used in those designs are right-handed in nature, i.e., with series inductance and shunt capacitance. The left-handed design is a dual structure and possesses some desirable properties. For example, its resonant frequency increases with the number of stages; while in right-handed structures, a longer ring leads to a lower resonant frequency. These make it more suitable for multi-phase signal generation at high frequencies. We will discuss this left/right-handed duality in the context of oscillator design in detail.

This structure can also be considered as capacitive coupling of LC oscillators. Along this line, [22], [23] presented similar structures to reduce phase noise or phase error. However, a thorough analysis of the oscillator's dynamics and phase noise performance in the presence of multiple resonant modes was still missing. We will address this using a mode-decomposition model: in a two-stage ring, the co-existence of two resonant modes leads to phase uncertainty unless additional active coupling is used; in LC-rings with more than two stages, the nonlinearity of negative resistors is enough to eliminate all but one resonant mode and thus enables well-defined multiple phases; the scaling of phase noise, as discussed above, is also derived based on the impulse sensitivity function (ISF) theory [24] and the mode-decomposition model.

In the rest, we will begin with a thorough study of various LC-ring structures in Section II. In Section III and Section IV, we will analyze the dynamics of two-stage and four-stage left-
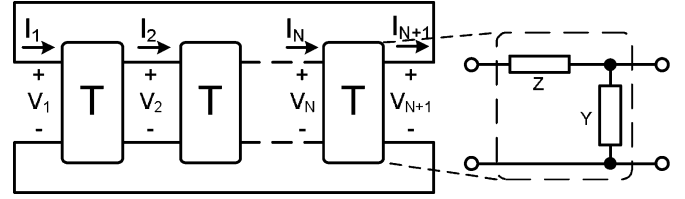
handed LC-rings in the context of quadrature oscillator design. Phase noise and phase error are discussed in Section V and Section VI, respectively. These analyses will be verified by prototype simulation and measurement in Section VII. Finally, we will conclude in Section VIII.

II. LC-RING: RESONANT MODE ANALYSIS

LC-ring is a high-order resonator that may have multiple resonant modes, i.e., several resonant frequencies and corresponding voltage/current patterns. We will study the resonance of various LC-rings and compare the duality of left- and right-handed structures.

A. Single-Ended LC-Ring

We start with a general artificial transmission line consisting of identical stages, as shown in Fig. 3. Each stage is a two-port network, with series impedance $Z(\omega)$ and shunt admittance $Y(\omega)$. It can be described by its transmission matrix (i.e. ABCD matrix) [25]

$$T(\omega) = \begin{bmatrix} 1 & Z(\omega) \\ 0 & 1 \end{bmatrix} \begin{bmatrix} 1 & 0 \\ Y(\omega) & 1 \end{bmatrix}$$
$$= \begin{bmatrix} 1 + Y(\omega)Z(\omega) & Z(\omega) \\ Y(\omega) & 1 \end{bmatrix}. \quad (2)$$

Cascading such stages, we get an artificial transmission line. On the one hand, the voltages and currents at successive stages are related by its transmission matrix, i.e.,

$$\begin{bmatrix} V_{n-1} \\ I_{n-1} \end{bmatrix} = T(\omega) \begin{bmatrix} V_n \\ I_n \end{bmatrix}. \quad (3)$$

On the other hand, for a wave propagating in this line, the voltages and currents must satisfy
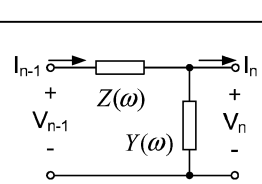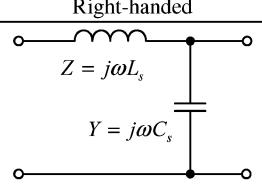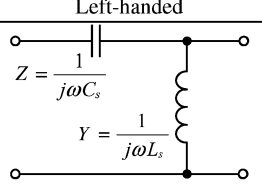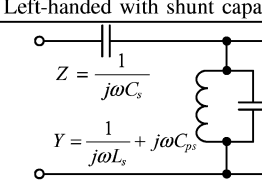
$$\begin{bmatrix} V_{n-1} \\ I_{n-1} \end{bmatrix} = e^{\alpha(\omega)+j\theta(\omega)} \begin{bmatrix} V_n \\ I_n \end{bmatrix} \quad (4)$$

where $\alpha(\omega)$ models the amplitude decay and $\theta(\omega)$ is the phase delay. $\alpha(\omega)$ and $\theta(\omega)$ are derived from $T(\omega)$ as follows [25]. A signal satisfying both (3) and (4) must also satisfy (3)–(4), that is,

$$\left(T(\omega) - e^{\alpha(\omega)+j\theta(\omega)} \begin{bmatrix} 1 & 0 \\ 0 & 1 \end{bmatrix} \right) \begin{bmatrix} V_n \\ I_n \end{bmatrix} = 0 \quad (5)$$

In order to have a nontrivial solution, the determinant of the above matrix must be zero, or, equivalently, $e^{\alpha(\omega)+j\theta(\omega)}$ must be an eigenvalue of $T(\omega)$. By this condition, one can find $\alpha(\omega) + j\theta(\omega)$ for a given $T(\omega)$, and the relation between $\alpha + j\theta$ and

TABLE I
COMPARISON OF SINGLE-ENDED LC-RINGS

	Right-handed	Left-handed	Left-handed with shunt capacitor
	$Z = j\omega L_s$ $Y = j\omega C_s$	$Z = \dfrac{1}{j\omega C_s}$ $Y = \dfrac{1}{j\omega L_s}$	$Z = \dfrac{1}{j\omega C_s}$ $Y = \dfrac{1}{j\omega L_s} + j\omega C_{ps}$
Dispersion Relation (i.e. $\theta - \omega$ Relation)	$\omega = 2\left\|\sin\frac{\theta}{2}\right\|\frac{1}{\sqrt{L_s C_s}}$	$\omega = \frac{1}{2\left\|\sin\frac{\theta}{2}\right\|}\frac{1}{\sqrt{L_s C_s}}$	$\omega = \frac{1}{\sqrt{C_{ps}/C_s + 4\sin^2\frac{\theta}{2}}}\frac{1}{\sqrt{L_s C_s}}$
Phase Shift per Stage $\theta^{(k)}$ for N-stage ring	$\frac{2k\pi}{N}$	$\frac{2k\pi}{N}$	$\frac{2k\pi}{N}$
Resonant Frequency $\omega^{(k)}$ of N-stage ring	$2\left\|\sin\frac{k\pi}{N}\right\|\frac{1}{\sqrt{L_s C_s}}$	$\frac{1}{2\left\|\sin\frac{k\pi}{N}\right\|}\frac{1}{\sqrt{L_s C_s}}$	$\frac{1}{\sqrt{C_{ps}/C_s + 4\sin^2\frac{k\pi}{N}}}\frac{1}{\sqrt{L_s C_s}}$
Characteristic Impedance $Z_0(\omega^{(k)}) = V_n/I_n$	$\frac{j2\left\|\sin\frac{k\pi}{N}\right\|}{1 - e^{-j\frac{2k\pi}{N}}}\sqrt{\frac{L_s}{C_s}}$	$-\frac{j2\left\|\sin\frac{k\pi}{N}\right\|}{1 - e^{-j\frac{2k\pi}{N}}}\sqrt{\frac{L_s}{C_s}}$	$-\frac{j\sqrt{C_{ps}/C_s + 4\sin^2\frac{k\pi}{N}}}{1 - e^{-j\frac{2k\pi}{N}}}\sqrt{\frac{L_s}{C_s}}$

ω is called the dispersion relation.[1] Then substituting the derived $\alpha(\omega) + j\theta(\omega)$ and solving (5), one can get V_n and I_n. Their ratio is the transmission line's characteristic impedance $Z_0(\omega) = V_n/I_n$, which is frequency-dependent.

If an N-stage transmission line forms a ring resonator as in Fig. 3, a periodic boundary condition should be imposed such that $V_1 = V_{N+1}$ and $I_1 = I_{N+1}$. Considering (4), one can find this boundary condition means $\alpha(\omega) = 0$ and the phase shift per stage can only be

$$\theta^{(k)} = \frac{2k\pi}{N}, \text{ with } k = \ldots, -1, 0, 1, \ldots.$$

Then, substituting these values into the dispersion relation $\alpha(\omega) + j\theta(\omega)$, one can solve all possible resonant frequencies $\omega^{(k)}$ of the ring resonator. Intuitively, the resonant frequency can only be such values that the total round-trip phase shift $N \cdot \theta(\omega)$ is an integer multiple of 2π.

Based on the above discussion, we can find the dispersion relation of the general artificial transmission line in Fig. 3, i.e. the $\theta - \omega$ relation, is governed by

$$Y(\omega)Z(\omega) = 2(\cos\theta - 1) \tag{6}$$

and its characteristic impedance is

$$Z_0(\omega) = \frac{V_n}{I_n} = \frac{Z(\omega)}{1 - e^{-j\theta(\omega)}}. \tag{7}$$

For an N-stage ring resonator, as the phase shift per stage can only be $\theta^{(k)} = (2k\pi/N)$, one can solve the corresponding resonant frequency $\omega^{(k)}$ after substituting $\theta^{(k)} = (2k\pi/N)$ into (6). Then, one can derive the corresponding characteristic impedance $Z_0(\omega^{(k)})$ from (7). Considering the periodicity of $\cos\theta$ in (6), one can find N possible resonant modes for an N-stage single-ended ring. It is also worth mentioning, because of the symmetry of the ring, wave can propagate both clockwise and counter-clockwise, which is predicted by the fact that (6) has the same solutions for $\theta^{(k)} = (2k\pi/N)$ and $\theta^{(-k)} = (-2k\pi/N)$. We consider them as two different modes at the
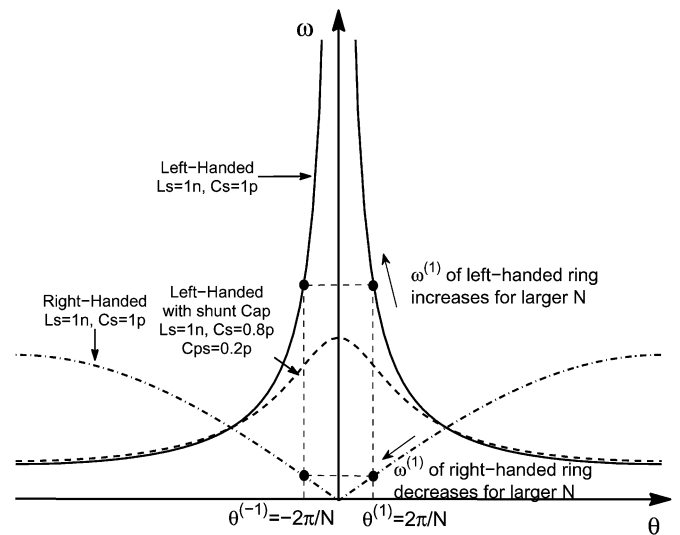

Fig. 4. Typical dispersion relations of right-handed and left-handed structures. For fair comparison, the total inductance and capacitance are the same for three structures.

same frequency. As shown later, coexistence of these two modes may cause poorly-defined phase relation in oscillators.

Next, we will discuss three typical structures, namely right-handed ring, left-handed ring and left-handed ring with shunt capacitance. Their schematics, dispersion relations, resonant frequencies and characteristic impedances are summarized in Table I. We also plot their dispersion relations in Fig. 4 for comparison. As mentioned before, the right-handed and the left-handed structures show duality [17], [18]. In particular,

- Dispersion relation: as illustrated in Fig. 4, for a right-handed cell, ω increases with $|\theta|$; while for a left-handed cell, ω decreases with $|\theta|$. As a result, for the resonant mode with $\theta^{(1)} = (2\pi/N)$, which, as to be shown later, is typically the working mode of an N-stage ring due to its low energy loss, the resonant frequency $\omega^{(1)}$ decreases with N in right-handed ring; while it increases in left-handed ring. This makes the left-handed structure more suitable for multi-phase high-frequency oscillators. As an illustration, if $N > 6$ and using the same inductance L and

---

[1]For each ω, there are two solutions of $\alpha + j\theta$, corresponding to waves in opposite directions and with the same $|\theta|$. But without causing confusion, we use $\theta(\omega)$ to emphasize the dependence between θ and ω. Similar is the case of $Z_0(\omega)$ below.
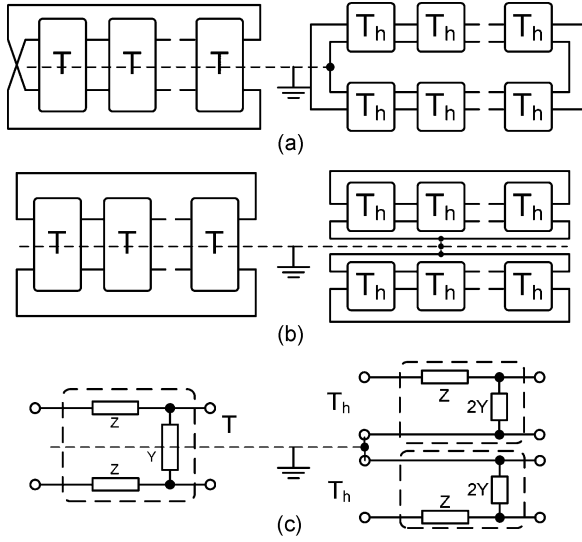
Fig. 5. Illustration of differential LC-rings and their equivalent single-ended models: (a) Mobius-connected ring, (b) non-mobius-connected ring and (c) the inner structure of each stage.

capacitance C, a left-handed ring has higher $\omega^{(1)}$ than a right-handed one.

- DC mode: the right-handed ring has a DC mode, that is the mode with $\theta^{(0)} = 0$ and $\omega^{(0)} = 0$. This is actually a stable DC state, in which all shunt capacitors take the same constant voltage and the series inductors carry zero current. Thereby, one must take measures in oscillator design to avoid the right-handed resonator being trapped in this DC state. In contrast, the left-handed ring does not have a DC mode with zero resonant frequency.

In reality, due to parasitic or intentionally-added shunt capacitance, the left-handed structure may turn to the third structure in Table I. It is quite similar to purely left-handed ring, except for the frequency shift caused by C_s, as shown by the dispersion relation in Fig. 4. Besides, the lowest mode corresponding to $\theta = 0$ exists and shows the highest resonance frequency $1/\sqrt{L_s C_{ps}}$.

B. Differential LC-Ring

Differential LC-ring is an extension to the single-ended LC-ring, and entails two ways of closing the loop, namely mobius and non-mobius connections as shown in Fig. 5. Generally, one can not treat the cell in Fig. 5(c) as a two-port network, since it has four terminals. However, under the assumption of differential operation, it is virtual ground at the center of the shunt admittance Y, from where we can break the cell into two two-port networks. After this splitting, an N-stage non-mobius differential ring reduces to two N-stage single-ended rings (Fig. 5(b)), but an N-stage mobius ring turns out to be one 2N-stage single-ended ring (Fig. 5(a)).

As a result, an N-stage non-mobius differential ring behaves exactly the same as an N-stage single-ended ring and the phase shift can be $\theta^{(k)} = (2k\pi/N)$. On the other hand, due to the constraint of differential operation, an N-stage mobius differential ring supports only N of the 2N modes of a 2N-stage single-ended ring, and the phase shift can only be $\theta^{(2k+1)} =$

$(2(2k+1)\pi/2N) = ((2k+1)\pi/N)$ such that the total phase shift of N stages is an odd multiple of π. To sum up, an N-stage differential ring has N resonant modes for both mobius and non-mobius connections, but the phase shift per stage is different for the two cases. In particular, a mobius ring does not allow the mode with $\theta^{(0)} = 0$, which is important to multi-phase oscillator design in that it rules out the mode with all stages resonating in phase as well as the DC mode of the right-handed structure.

In addition, as two identical single-ended inductors in series can be readily implemented as one center-tapped symmetric inductor, a left-handed differential ring can save half of the inductors needed for a right-handed ring of the same length and thus has a more compact layout.

C. Mode Selection

In most applications, we want the oscillator to work in a certain mode, so as to generate a desired frequency and phase relation. Essentially, mode selection relies on energy loss and compensation. Only the modes that can get enough energy compensation can survive. Next, we will analyze two examples to illustrate the mode-selection mechanism.

First, consider a single-ended right-handed ring, as shown in Fig. 6. Assume energy loss is mainly from the series resistance of inductor and capacitor, i.e., R_{LS} and R_{CS}. Under the assumption of high Q, the loss can be modeled by a shunt resistor R_P satisfying [7]

$$\frac{|V_2|^2}{R_P} = |V_2|^2 \omega^2 C_s^2 R_{Cs} + \frac{|V_1 - V_2|^2}{\omega^2 L_s^2} R_{Ls}. \qquad (8)$$

According to Table I, for a resonant mode with phase shift $\theta^{(k)}$ in a right-handed ring, we have $V_1 = e^{j\theta^{(k)}} V_2$ and $\omega^{(k)} = 2|\sin(\theta^{(k)}/2)|(1/\sqrt{L_s C_s})$. Thus, $R_P = (L_s/(C_s(R_{Ls} + 4\sin^2(\theta^{(k)}/2)R_{Cs})))$. Clearly, smaller $|\theta^{(k)}|$ leads to larger R_P and thus less energy loss. A similar analysis shows, for left-handed ring, a mode with smaller $|\theta^{(k)}|$ also has less loss. Therefore, by properly setting the negative resistor $-R$, we can damp the high-loss modes and end up with the mode with the least loss. As an illustration, we simulated a left-handed and a right-handed ring in a 0.13 μm CMOS process. Both are four-stage mobius-connected differential rings. Fig. 7 shows the input impedances measured from the two terminals of a shunt admittance, i.e., where negative resistor is usually connected. As expected, two peaks appear in each curve, corresponding to resonant modes with $\theta^{(\pm 1)} = \pm(\pi/4)$ and $\theta^{(\pm 3)} = \pm(3\pi/4)$, respectively. In both cases, the modes with $\theta^{(\pm 1)} = \pm(\pi/4)$ show higher impedance and less loss than those with $\theta^{(\pm 3)} = \pm(3\pi/4)$. Therefore, an oscillator tends to work at the modes with $\theta^{(\pm 1)} = \pm(\pi/4)$ in both cases. However, $\theta^{(\pm 1)} = \pm(\pi/4)$ corresponds to the high frequency mode in the left-handed ring, but the low frequency mode in the right-handed ring.

A second example in Fig. 8 shows the role of active devices. Considering the parasitic capacitors, it can be recognized as a four-stage single-ended left-handed LC-ring with shunt capacitors. There are four modes, with $\theta = 0$, $\pm(\pi/2)$ and π, respectively. For $\theta^{(0)} = 0$, the drain voltage and drain current of MOSFETs are in phase, which adds to the energy loss of the LC
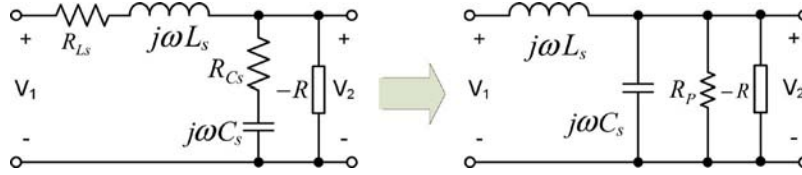
Fig. 6. Equivalent circuit for energy loss calculation of single-ended right-handed LC-ring.
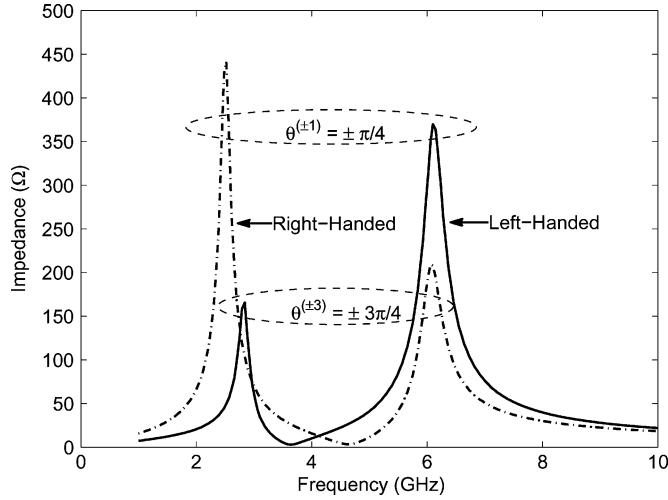

Fig. 7. Input impedances of left-handed and right-handed LC-rings in a 0.13 μm CMOS process. Both have four stages and are mobius-connected. Impedances are measured from the two terminals of a shunt admittance. The same inductor is used in the two rings, and capacitors are tuned such that the resonant frequencies align.
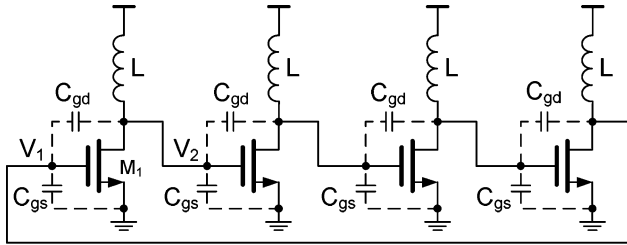

Fig. 8. Mode selection through active devices in a four-stage single-ended left-handed LC-ring oscillator.

ring; for $\theta^{(\pm 1)} = \pm(\pi/2)$, the drain voltage and current are in quadrature, which only resonates and does not inject net energy into the LC ring; for $\theta^{(2)} = \pi$, the drain voltage and current are opposite in sign, which leads to net energy injection. Therefore, only the last mode can survive.

To sum up, a left-handed mobius ring, as illustrated in Fig. 2, resonates at its highest-frequency mode, uses less inductors than right-handed ring, and its frequency increases with the number of stages/phases. Thereby, it is suitable for multi-phase oscillator at high frequencies.

III. Two-Stage LC-Ring Oscillator

Based on Section II-B, the two-stage left-handed mobius LC-ring in Fig. 9 is equivalent to a four-stage single-ended ring, but only supports two of its four resonate modes with

$\theta^{(\pm 1)} = \pm(\pi/2)$. Although this ring seems promising to generate quadrature signal, we will show coexistence of these two modes causes poorly-defined phase relation, unless coupling transistors are used between the two stages to damp one of the two modes.

It is straightforward to derive the characteristics of the two-stage mobius ring in Fig. 9 from its four-stage single-ended equivalent circuit based on Table I. Specifically, substituting $N = 4$, $k = \pm 1$, $L_s = L/2$, $C_{ps} = 2C_p$, $C_s = C$ into the last column of Table I, one can get the two resonant modes are at the same frequency $\omega^{(1)} = \omega^{(-1)} = \omega_0 = (1/\sqrt{L(C + C_P)})$; the characteristic impedance $Z_0(\omega) = V_n/I_n$ of the differential line are twice the single-ended one, i.e.,

$$Z_0\left(\omega^{(1)}\right) = -(1+j)\frac{\sqrt{L(C_P + C)}}{C}, \qquad (9)$$

$$Z_0\left(\omega^{(-1)}\right) = (1-j)\frac{\sqrt{L(C_P + C)}}{C}. \qquad (10)$$

Considering $V_1 = e^{j\theta}V_2$, $I_1 = e^{j\theta}I_2$ and $Z_0 = V_n/I_n$, we can find the voltage/current patterns of the two resonant modes are

$$\text{Mode}^{(1)} = \begin{bmatrix} V_1 \\ I_1 \\ V_2 \\ I_2 \end{bmatrix}^{(1)} = \begin{bmatrix} j \\ A(-1-j) \\ 1 \\ A(-1+j) \end{bmatrix}, \qquad (11)$$

$$\text{Mode}^{(-1)} = \begin{bmatrix} V_1 \\ I_1 \\ V_2 \\ I_2 \end{bmatrix}^{(-1)} = \begin{bmatrix} -j \\ A(1-j) \\ 1 \\ A(1+j) \end{bmatrix}, \qquad (12)$$

where $A = C/2\sqrt{L(C + C_P)}$ and the two vectors are normalized such that $V_2 = 1$. A superposition of the two modes, denoted by $m \cdot \text{Mode}^{(1)} + jn \cdot \text{Mode}^{(-1)}$, produces port voltages $V_1 = n + jm$ and $V_2 = m + jn$. It is easy to check, V_1 and V_2 have the same amplitude but can have arbitrary phase relation, depending on m and n. Therefore, only one mode can exist in order to generate well-defined quadrature signals.

Next, we will study the dynamics of the two modes in oscillator and look for ways of mode selection. As illustrated in Fig. 9 and Fig. 10, the oscillator consists of two parts:

1) LC-ring. It can be modeled as a two-input two-output linear time-invariant (LTI) system $H(s)$, with currents $[i_{P1}, i_{P2}]$ as its input and voltages $[v_1, v_2]^2$ as its output. Under differential operation, it is a fourth-order system, in that the states of all energy-storing components can be uniquely represented by four independent variables. They can be $[v_1, i_1, v_2, i_2]$. Alternatively, they can be the complex amplitudes of the two resonant modes,

---

[2]We use lower-case v or i to denote a time-domain signal, and upper-case for the phasor of the same signal.
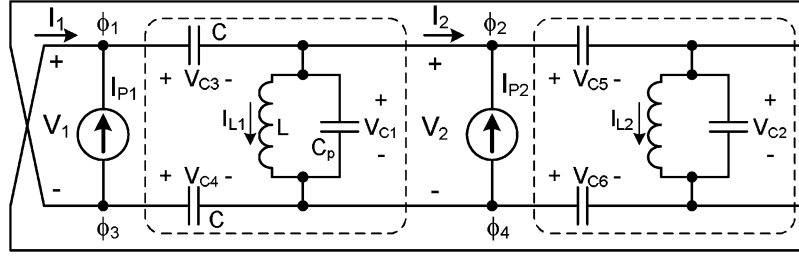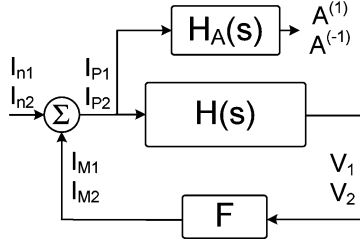
Fig. 9. Illustration of two-stage left-handed mobius LC-ring oscillator.

Fig. 10. Mathematical model of the two-stage left-handed LC-ring oscillator in Fig. 9. The LC-ring is modeled as a two-input two-output LTI network $H(s)$ or equivalently $H_A(s)$. The transconductance network F converts voltages $[V_1, V_2]$ into currents $[I_{P1}, I_{P2}]$.

i.e., $A^{(1)} = |A^{(1)}|e^{j\phi^{(1)}}$ and $A^{(-1)} = |A^{(-1)}|e^{j\phi^{(-1)}}$. These two sets of variables have a one-to-one correspondence given by

$$\begin{bmatrix} v_1 \\ i_1 \\ v_2 \\ i_2 \end{bmatrix} = Re\left\{ \left|A^{(1)}\right| e^{j\phi^{(1)}} \cdot \text{Mode}^{(1)} \right.$$
$$\left. + \left|A^{(-1)}\right| e^{j\phi^{(-1)}} \cdot \text{Mode}^{(-1)} \right\}. \quad (13)$$

This mode decomposition provides a convenient way to study state evolution, as each mode goes at its own resonate frequency. For instance, we will study zero-state impulse responses. Consider a current impulse injected from $i_{P1} = \delta(t)$. It is easy to find, at $t = 0^+$, $i_{L1} = i_{L2} = 0$, $v_{C1} = 0$, $v_{C2} = -(1/(C + C_P))$, $v_{C3} = v_{C5} = (1/2(C + C_P))$ and $v_{C4} = v_{C6} = -(1/2(C + C_P))$. It is equivalent to,

$$\begin{bmatrix} v_1 \\ i_1 \\ v_2 \\ i_2 \end{bmatrix}_{I_{P1}} (0^+) = \begin{bmatrix} \frac{1}{(C+C_P)} \\ 0 \\ 0 \\ 0 \end{bmatrix}$$
$$= Re\left\{ \frac{-j}{2(C + C_P)} \cdot \text{Mode}^{(1)} \right.$$
$$\left. + \frac{j}{2(C + C_P)} \cdot \text{Mode}^{(-1)} \right\}. \quad (14)$$

As the two modes evolve at their own resonate frequencies, the impulse response to i_{P1} is

$$\begin{bmatrix} v_1 \\ i_1 \\ v_2 \\ i_2 \end{bmatrix}_{I_{P1}} (t) = Re\left\{ \frac{-j}{2(C + C_P)} e^{j\omega^{(1)}t} \cdot \text{Mode}^{(1)} \right.$$
$$\left. + \frac{j}{2(C + C_P)} e^{j\omega^{(-1)}t} \cdot \text{Mode}^{(-1)} \right\}. \quad (15)$$

Similarly, the zero-state impulse response to $i_{P2} = \delta(t)$ is found to be

$$\begin{bmatrix} v_1 \\ i_1 \\ v_2 \\ i_2 \end{bmatrix}_{I_{P2}} (t) = Re\left\{ \frac{1}{2(C + C_P)} e^{j\omega^{(1)}t} \cdot \text{Mode}^{(1)} \right.$$
$$\left. + \frac{1}{2(C + C_P)} e^{j\omega^{(-1)}t} \cdot \text{Mode}^{(-1)} \right\}. \quad (16)$$

Considering $\omega^{(1)} = \omega^{(-1)} = \omega_0$, we conclude the zero-state response of $A^{(1)}(t)$ and $A^{(-1)}(t)$ is

$$\begin{bmatrix} A^{(1)}(t) \\ A^{(-1)}(t) \end{bmatrix} = \frac{e^{j\omega_0 t}u(t)}{2(C + C_P)} * \begin{bmatrix} -j & 1 \\ j & 1 \end{bmatrix} \begin{bmatrix} i_{P1}(t) \\ i_{P2}(t) \end{bmatrix} \quad (17)$$

where '$*$' stands for convolution, and $u(t) = 1$ for $t > 0$ and 0 elsewhere. Thus, the transfer function from $[i_{P1}, i_{P2}]$ to $[A^{(1)}, A^{(-1)}]$ is given by

$$H_A(s) = \frac{1}{2(C + C_P)} \frac{1}{s - j\omega_0} \begin{bmatrix} -j & 1 \\ j & 1 \end{bmatrix} \quad (18)$$

Similarly, the transfer function from $[i_{P1}, i_{P2}]$ to $[v_1, v_2]$, i.e., $H(s)$ in Fig. 10, is found to be

$$H(s) = \frac{1}{(C + C_P)} \frac{s}{s^2 + \omega_0^2} \begin{bmatrix} 1 & 0 \\ 0 & 1 \end{bmatrix}. \quad (19)$$

2) A transconductance network converting $[v_1, v_2]$ into $[i_{P1}, i_{P1}]$. It describes all the active devices, as well as the energy loss of the LC-ring, like R_P in Fig. 6. It can be modeled as

$$\begin{bmatrix} i_{P1} \\ i_{P2} \end{bmatrix} = \begin{bmatrix} i_{n1} \\ i_{n2} \end{bmatrix} + F \begin{bmatrix} v_1 \\ v_2 \end{bmatrix} = \begin{bmatrix} i_{n1} \\ i_{n2} \end{bmatrix} + \begin{bmatrix} g_m & -g_c \\ g_c & g_m \end{bmatrix} \begin{bmatrix} v_1 \\ v_2 \end{bmatrix} \quad (20)$$

where g_m is the local conductance, including the negative resistor and the energy loss R_P of the LC resonator, g_c is the cross-coupling transconductance, and $[i_{n1}, i_{n2}]$ are electronic noises.

Then, the response of the two modes $[A^{(1)}, A^{(-1)}]$ to the input $[I_{n1}, I_{n2}]$ can be found to be

$$\begin{bmatrix} A^{(1)}(s) \\ A^{(-1)}(s) \end{bmatrix} = H_A(s) [I - FH(s)]^{-1} \cdot \begin{bmatrix} I_{n1}(s) \\ I_{n2}(s) \end{bmatrix}$$
$$= \begin{bmatrix} H_{A^{(1)}}(s) \cdot [-jI_{n1}(s) + I_{n2}(s)] \\ H_{A^{(-1)}}(s) \cdot [jI_{n1}(s) + I_{n2}(s)] \end{bmatrix} \quad (21)$$

in which

$$H_{A^{(1)}}(s) = \frac{1}{2(C+C_p)} \cdot \frac{s+j\omega_0}{s^2 - \frac{g_m+jg_c}{C+C_p}s + \omega_0^2} \qquad (22)$$

$$H_{A^{(-1)}}(s) = \frac{1}{2(C+C_p)} \cdot \frac{s+j\omega_0}{s^2 - \frac{g_m-jg_c}{C+C_p}s + \omega_0^2} \qquad (23)$$

can be considered as the transfer functions from the input noise to the two resonant modes. It is easy to check, the poles of $H_{A^{(1)}}(s)$ and $H_{A^{(-1)}}(s)$ have different real parts only if g_c has a non-zero imaginary part. That is, only by using cross-coupling transconductance with phase delay, we can start one mode while damp the other. This is the same as cross-coupled quadrature oscillators using two independent LC tanks, where active coupling is necessary [10], [28]. Coupling MOSFETs has inherent delay from gate voltage to drain current, due to parasitics and the non-quasi-static behavior of the channel [7], making quadrature oscillation possible. However, as this delay is usually much smaller than $90°$, coupling MOSFETs mainly act as active reactance which deteriorates phase noise performance as discussed in Section I.

To sum up, the two-stage LC-ring in Fig. 9 is quite similar to two independent LC tanks, and active coupling between two-stages is necessary for quadrature generation. Therefore, it suffers the same trade-off between phase error and phase noise as cross-coupled quadrature oscillators.

IV. FOUR-STAGE RING OSCILLATOR

We move on to the four-stage LC-ring (Fig. 2 with $N = 4$) to look for quadrature oscillator design. In the same way as Section III, we can find it has four resonance modes, with $\theta^{(\pm1)} = \pm(\pi/4)$ and $\theta^{(\pm3)} = \pm(3\pi/4)$, respectively. Their resonant frequencies can be derived from Table I as

$$\omega^{(\pm1)} = 1/\sqrt{L\left(C_p + (1-1/\sqrt{2})C\right)} \qquad (24)$$

$$\omega^{(\pm3)} = 1/\sqrt{L\left(C_p + (1+1/\sqrt{2})C\right)}. \qquad (25)$$

Again, it is easy to check, in order to generate quadrature signals, only one mode can exist. Fortunately, we can achieve this through two mechanisms without extra active coupling devices.

First, as discussed in Section II-C, the modes with $\theta^{(\pm1)} = \pm(\pi/4)$ have less energy loss, and we can eliminate the two modes with $\theta^{(\pm3)} = \pm(3\pi/4)$ by setting the negative resistor properly. To get a quantitative idea, assume the series resistor R_s of the inductor dominates energy loss. Under the assumption of high Q, it is equivalent to a parallel resistor $R_p(\omega) = \omega^2 L^2/R_s$, as illustrated in Fig. 11. In the case of $C_p = C$, we find $\omega^{(\pm3)} \approx 0.7\omega^{(\pm1)}$ and $R_p(\omega^{(\pm3)}) \approx 0.5 \times R_p(\omega^{(\pm1)})$. For a large design margin for $-R$, one should separate $\omega^{(\pm1)}$ and $\omega^{(\pm3)}$ apart by using large C and small C_p. That is, C_p should use the smallest varactor that achieve the desired tuning range. Generally, this mechanism rules out all but the two modes with $\theta^{(\pm1)}$ in an N-stage mobius ring.

The second mode-selection mechanism happens when the negative resistors enter nonlinear region and the oscillator goes into steady oscillation. The oscillation amplitude saturates due to the nonlinearity of negative resistors and the voltages at the
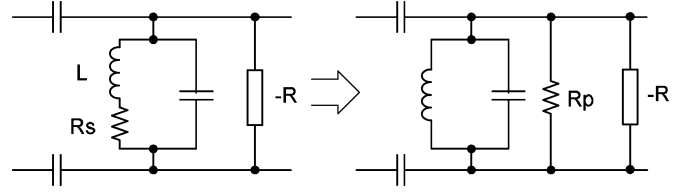

Fig. 11. Equivalent circuit for energy loss calculation of left-handed cell.

four ports tend to have the same amplitude, provided the same negative resistor is used and/or the oscillator is in voltage-limited region [31]. In this case, the resonator stores the most energy and thus dissipates the largest power that the negative resistors can compensate. However, if both modes with $\theta^{(\pm1)} = \pm(\pi/4)$ exist, a standing wave forms and it can not have the same amplitude at all four LC tanks, as illustrated in Fig. 12. Though complicated nonlinear dynamics gets involved, we can conclude only one mode can survive in the end, such that all the four ports have the same amplitude. Actually, this mechanism works for any mobius ring longer than two stages. This is because, for $N > 2$ and phase shift $\theta^{(\pm1)} = \pm(\pi/N)$, there is not such non-zero coefficients a and b that the superposition $|V_n| = |a \cdot e^{jn\theta^{(1)}} + b \cdot e^{jn\theta^{(-1)}}| = |a||1 + (b/a)e^{-j2n\pi/N}|$ has the same amplitude for all the N stages, i.e., for all $n = 0, \cdots, N-1$. But in the case of $N = 2$, such superposition exists, e.g., $a = 1$ and $b = j$, and thereby this mechanism can not dissolve the mode-coexistence problem in a two stage ring. Furthermore, if a definite phase order is required, a small asymmetry can be introduced to the ring to make a preference between $\theta^{(1)} = (\pi/N)$ and $\theta^{(-1)} = -(\pi/N)$.

Thus, the two mechanisms damps all but one mode without extra active coupling devices.

V. PHASE NOISE

Phase noise is a primary concern in oscillator design, and extensive studies have been done on the general theory [24], [32] as well as the two most widely used oscillator structures, i.e., differential LC oscillator [29], [31] and active ring oscillator [33], [34]. The presented LC-ring oscillator is a natural extension to the differential LC oscillator, which is actually a single-stage LC-ring, and the noise injection mechanisms are quite similar for the two. So, most analysis and noise-reducing techniques developed for single-stage LC oscillators can be readily adopted here. In this section, we are going to study how phase noise scales with the length of the LC-ring.

Consider an N-stage LC-ring oscillator, as shown in Fig. 2. It has N possible resonant modes, and in steady operation, it assumes one of them as its working mode. Suppose a current pulse is injected into the LC-ring at $t = \tau$. In the same way as (14), the response of the LC-ring can be decomposed into all its N resonant modes,[3] with complex amplitudes $\Delta A^{(k)} = |\Delta A^{(k)}|e^{j\phi^{(k)}}$, $k = 1, \cdots, N$, respectively. While $N-1$ of these components appear as amplitude noise and decay fast, the component on the working mode of the oscillator, say $\Delta A^{(1)}$, will persist and perturb the phase of oscillation by changing its original complex amplitude $A^{(1)}(\tau)$ into $A^{(1)}(\tau) + \Delta A^{(1)}$. The

---

[3]Assume all modes are normalized and each have unit energy in this section.
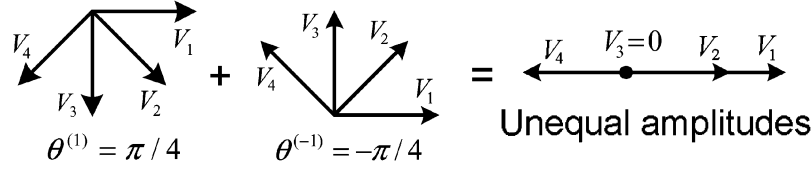
Fig. 12.   Co-existence of two modes leads to standing wave and unequal voltage amplitudes.
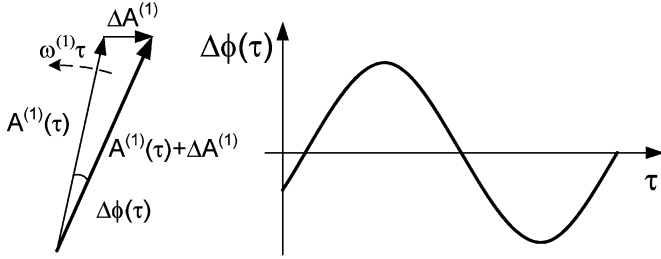

Fig. 13.   Illustration of oscillation phase perturbation from impulse injection.

phase shift $\Delta\phi(\tau)$ due to this current pulse is thus given by the angle between $A^{(1)}(\tau)$ and $A^{(1)}(\tau) + \Delta A^{(1)}$. As illustrated in Fig. 13, since $A^{(1)}(\tau)$ evolves at angular frequency $\omega^{(1)}$, $\Delta\phi(\tau)$ depends on when the pulse is injected, which indicates the periodic variation of the oscillator's phase sensitivity to noise injection. This is actually the impulse sensitivity function (ISF) in Hajimiri's phase noise theory [24], and, for high-Q LC resonator, $\Delta\phi(\tau)$ can be well approximated by a sinusoid function [26]. For noise much smaller than the oscillation swing, the amplitude of $\Delta\phi(\tau)$ can be shown to be proportional to the ratio $|\Delta A^{(1)}|/|A^{(1)}|$.

On the one hand, by equipartition theorem, each of the N resonance modes gets $1/N$ of the injected noise energy, which means $|\Delta A^{(1)}|^2$ is proportional to $1/N$; on the other hand, the total resonance energy of the LC-ring is proportional to N, i.e., $|A^{(1)}|^2$ is proportional to N. Thus, we find $\Delta\phi \propto |\Delta A^{(1)}|/|A^{(1)}| \propto 1/N$. That is, $\Delta\phi$ is proportional to $1/N$.

Based on the above discussion, we can expect the impulse sensitivity function (ISF) [24] of the LC-ring oscillator to be proportional to $1/N$. Considering the number of noise sources increases linearly with N, the total phase noise should be proportional to $N \cdot (1/N)^2 = 1/N$. Finally, as the power consumption is proportional to the number of stages N, the FoM as defined in (1) does not change with N. That is, an LC-ring oscillator can synthesize multiple phases while maintaining the high FoM of a single-stage LC oscillator. This also provides a systematic way of trading power for phase noise, especially in low-supply-voltage applications where the small voltage swing puts a limit on the minimum achievable phase noise with a single LC tank. Besides, as a natural extension to single-ended LC oscillator, the LC-ring oscillator can readily adopt many noise-reduction techniques developed for single-stage LC oscillators.

Interestingly, the FoM of an active ring oscillator does not change with its number of stages either, though its power consumption and phase noise scale differently from the LC-ring oscillator [33]. In this sense, the FoM indicates the best one can do with a given design of delay cell.
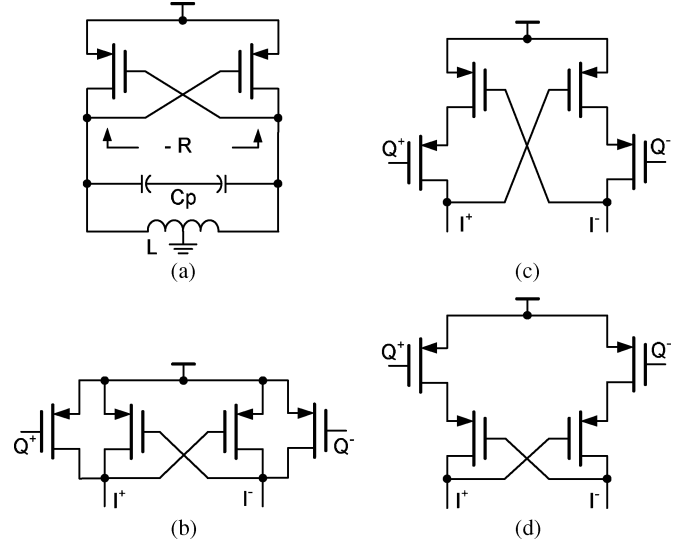

Fig. 14.   Prototype implementation details: (a) single-stage LC oscillator, the same negative resistor and inductor are also used in the four-stage LC-ring oscillator; (b) parallel coupling used in two-stage ring, (c) top-series coupling used in two-stage ring, and (d) bottom-series coupling used in two-stage ring. For two stage rings, the connections at Q stage are similar to I stage.

VI. PHASE ERROR

Phase error is another important specification of multi-phase oscillator. As mentioned earlier, the cross-coupled quadrature oscillator [8] uses MOSFETs to couple several independent LC tanks. But for the sake of phase noise, the coupling MOSFETs only carry a much smaller current than the LC tanks, which makes the coupling very weak. So, device mismatch would lead to large phase error. In this proposed LC-ring structure, the inductors and capacitors form a single resonator, capable of generating multiple phases. From another view, the current in the capacitors between LC tanks is comparable to the LC tanks, which make the coupling much stronger. Thus, we expect a much smaller phase error. This is verified in Section VII.

VII. PROTOTYPE AND EXPERIMENTS

To verify the above analysis, using a $0.13\ \mu$m CMOS process with 0.5 V supply voltage, we implemented the left-handed LC-ring oscillator in Fig. 2 with one, two and four stages, respectively. For fair comparison, the same symmetric inductor, using two top metals, is utilized in all oscillators. As illustrated in Fig. 14(a), the center tap of the inductor is connected to the ground, which provides DC bias for the negative resistor. All capacitors are implemented as metal-insulator-metal (MIM) capacitors and their values are tuned so that all oscillators are at around 5.4 GHz. The one- and four-stage oscillators use the same negative resistor as shown in Fig. 14(a), in which the

TABLE II
SUMMARY OF SIMULATION RESULTS

|	One Stage	Two-Stage parallel	Two-Stage top-series	Two-Stage bottom-series	Four Stage
V_{DD} (V)	0.5	0.5	0.5	0.5	0.5
I_{DC} (mA)	1.97	6.37	2.93	6.01	7.89
f_0 (GHz)	5.48	5.49	5.47	5.48	5.37
$L(\Delta f)$ (dBc/Hz@Hz)	-99.25@100k -115.3@600k -119.8@1M	-91.84@100k -114.0@600k -119.6@1M	-99.70@100k -116.4@600k -120.9@1M	-99.36@100k -117.0@600k -121.7@1M	-104.8@100k -121.5@600k -126.0@1M
FoM(Δf) (dB@Hz)	194.1@100k 194.6@600k 194.6@1M	181.6@100k 188.2@600k 189.4@1M	192.8@100k 193.9@600k 194.0@1M	189.4@100k 191.4@600k 191.7@1M	193.4@100k 194.6@600k 194.6@1M
I/Q Phase Error (active mismatch)	–	0.96^o	0.84^o	4.62^o	0.29^o
I/Q Phase Error (0.1% L mismatch)	–	1.27^o	0.23^o	1.56^o	0.10^o
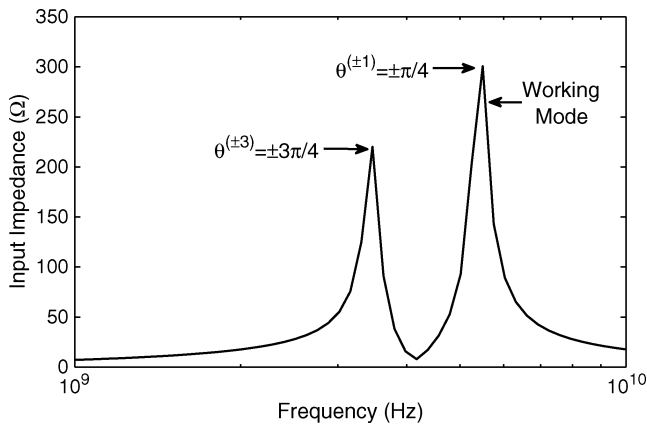
Fig. 15. Simulated input impedance of the four-stage LC-ring, seen by each negative resistor $-R$. The higher peak corresponds the resonant modes with $\pm\pi/4$ phase shift per stage, and has lower loss than the other peak.
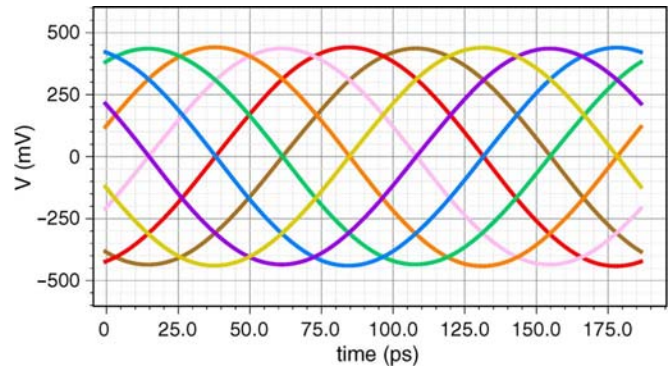

Fig. 16. Simulated voltage waveforms of at $\phi_1 - \phi_8$ (Fig. 2) of the four-stage LC-ring oscillator. Each stage has a phase shift of $\pi/4$ (45°).

aspect ratio of PFETs is $W/L = 72\ \mu\text{m}/0.12\ \mu\text{m}$. The negative conductance turns out to be 1.75 times the input conductance of the LC tank at resonance, which guarantees reliable start-up; it also puts the oscillator just in the voltage-limited region and leads to the best phase noise performance [31].

The design of active parts for two-stage LC-ring is more complicated, and various coupling structures have been proposed, such as parallel [8] and top-/bottom-series (TS/BS) [26] couplings. A fair comparison of those structures, with various configurations, is far from trivial and has been the topic of several previous publications [26], [27]. We will only show one scenario as an example. As illustrated in Fig. 14, we scale PFETs such that all three structures provide the same negative resistance as the one in the single-stage oscillator. As to the ratio between coupling and local MOSFETs, we use a typical value of 0.3 for parallel and 5 for series coupling [26].

A. Simulation Results

All five oscillators are simulation with SpectreRF, and the results are summarized in Table II. In particular, to verify the functionality of the four-stage LC-ring oscillator, we first set the supply voltage VDD to zero and simulate the impedance looking into ϕ_1 and ϕ_5 in Fig. 2, i.e., the impedance seen by "-R". The result is plotted in Fig. 15. As expected, there are two peaks, one

at 5.4 GHz and the other at 3.5 GHz. They correspond to resonant modes with $\theta = \pm(\pi/4)$ and $\pm(3\pi/4)$, respectively. Since at these frequencies inductors dominate in energy loss, the high frequency mode shows larger impedance, and thus less energy loss. Therefore, we expect the oscillator to work at around 5.4 GHz. Then, we set VDD to 0.5 V and run periodic steady-stage (pss) analysis with SpectreRF. It oscillates at 5.37 GHz. The voltages at $\phi_1 - \phi_8$ are plotted in Fig. 16, which shows eight equally-spaced phases with a phase shift of $\pi/4$.

To compare phase noise, we simulated ISFs of all five oscillators. Fig. 17 shows the simulated ISFs of net ϕ_1 (Fig. 2), which is the most sensitive net to noise injection. All curves have near-zero DC values and their root-mean-square (rms) values are calculated as their amplitudes. It is shown that the rms values are inversely proportional to the number of stages N: the four-stage one is exactly one-fourth of the one-stage one; the two-stage cases deviate a little, which is due to the additional coupling transistors. The ISFs at other nets show the same scaling ratio.

The simulated phase noises are plotted in Fig. 18 and the FoMs at different offset frequencies are compared in Table II. Specifically, there is a constant 6 dBc/Hz phase-noise gap between the one-stage and the four-stage oscillators for offset frequency larger than 100 kHz, which verifies the phase noise is inversely proportional to the number of stages N. Considering the power consumption of the four-stage oscillator is four time that of the one-stage case, they achieve the same FoM. As to
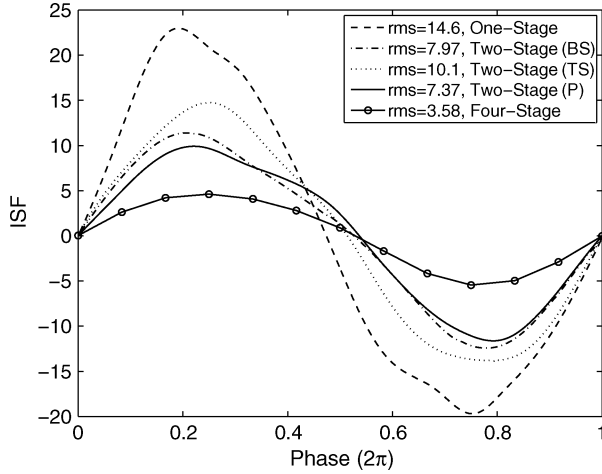
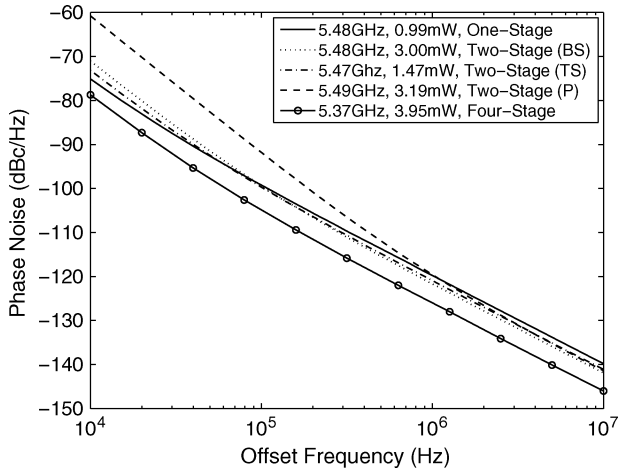Fig. 17. Simulated impulse sensitivity function (ISF) by SpectreRF.

Fig. 18. Simulated phase noise by SpectreRF. The four-stage LC-ring oscillator is 6 dBc/Hz lower than the one-stage oscillator. The two-stage oscillators show higher phase noise, due to coupling MOSFETs.
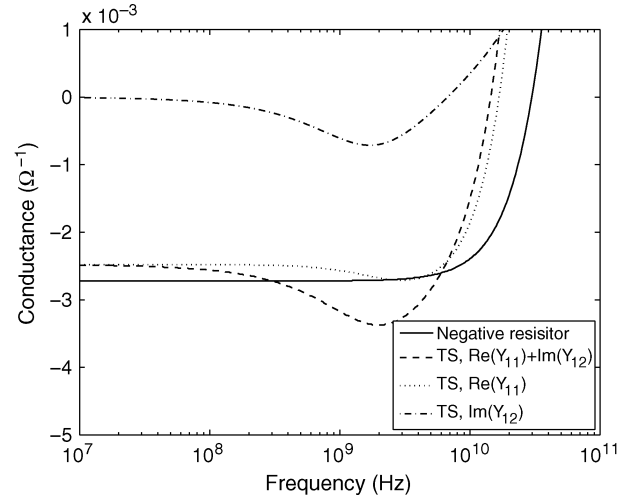

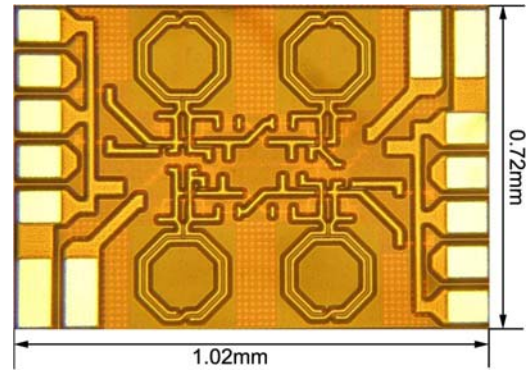Fig. 19. Frequency responses of top-series coupling structure in Fig. 14(c) and negative resistor in Fig. 14(a).

Fig. 20. Die micrograph of the four-stage LC-ring quadrature oscillator.

the two-stage rings, the three structures draw different currents and show different phase noises. But generally, due to additional noises from coupling MOSFETs, the phase noises are higher than they "should" be and their FoMs are lower than the single-stage one. In particular, parallel coupling structure shows significant flicker noise up-conversion. The two series-coupling structures show better phase noise performance and much lower flicker noise up-conversion than the parallel structure, which can be partially attributed to the large gate area of the coupling MOSFETs. We also did similar phase noise simulations in a 65 nm CMOS process, in which the negative resistors were implemented as complementary PFET and NFET pairs. It showed the same comparison result as above.

Phase error is largely a random event resulting from mismatch in active and passive devices. For active device mismatch, we derived the standard deviation of phase error from 500-point Monte Carlo simulations, in which the mismatch is specified by the process; while for passive mismatch, we simulated the phase error due to 0.1% inductor mismatch. The results are summarized in the last two rows of Table II. In both cases, the four-stage ring, which does not rely on active coupling, shows

much smaller phase error than the two-stage rings, which relies on active coupling. Therefore, we expect a better phase accuracy for the four-stage LC-ring oscillator.

As a final remark, the two series coupling structures introduce much larger parasitic capacitance than parallel coupling, which potentially reduces the tuning range of oscillator [27]. Besides, their frequency responses limit their application at high frequencies. As an illustration, the top-series structure is simulated as a two-port network, with $I^+ - I^-$ as port1 and $Q^+ - Q^-$ as port2. Along the same line as Section III, both $Re(Y_{11})$ and $Im(Y_{12})$ contribute to the negative conductance at port1. They are plotted in Fig. 19, along with the input conductance of the negative resistor in Fig. 14(a). Both fail to be a negative resistor as frequency goes up, but the negative resistor in Fig. 14(a) has a flat frequency response and works to much higher frequencies. Thereby, the four-stage LC-ring structure is more suitable for high-frequency applications.

B. Measurement Results

We fabricated the one-stage, four-stage and parallel-coupled two-stage LC-ring oscillators in a 0.13 μm CMOS process and did testing using Agilent 8564EC spectrum analyzer. The results are summarized in Table III. For phase noise, we repeated the measurement for ten times for each oscillator, and take the

TABLE III
SUMMARY OF MEASUREMENT RESULTS

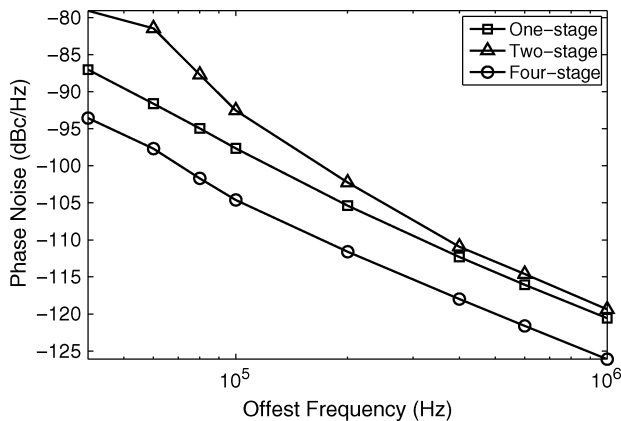|	One Stage	Two-Stage parallel	Four Stage
V_{DD} (V)	0.504	0.507	0.506
I_{DC} (mA)	2.01	5.18	8.01
f_0 (GHz)	5.341	5.410	5.121
$L(\Delta f)$ (dBc/Hz@Hz)	-97.7@100k -116.1@600k -120.6@1M	-92.5@100k -114.6@600k -119.4@1M	-104.6@100k -121.6@600k -126.1@1M
FoM(Δf) (dB@MHz)	192.2@100k 194.8@600k 195.1@1M	183.0@100k 189.4@600k 189.8@1M	192.7@100k 194.2@600k 194.2@1M
Phase Error	–	$1.9°$	$0.1°$

Fig. 21. Measured phase noise of the one-, two- and four-stage LC-ring oscillators. The four-stage oscillator shows a phase noise 6 dBc/Hz lower than the one-stage oscillator; the parallel-coupling two-stage one shows the highest phase noise.
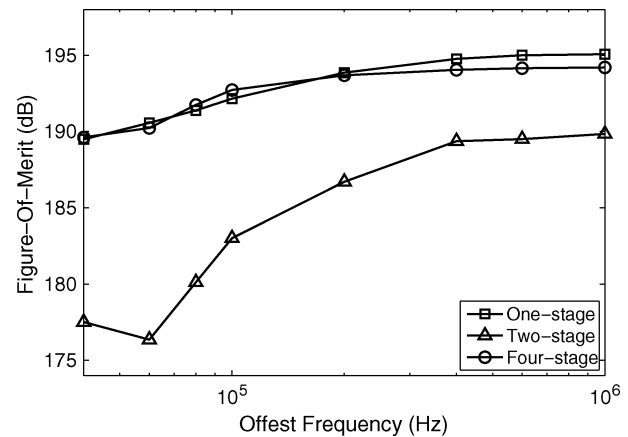

Fig. 22. Measured FoM of the one-, two- and four-stage left-handed LC-ring oscillators. The four-stage oscillator achieve the same FoM as the one-stage oscillator; the parallel-coupling two-stage one is 5–10 dB lower.

average values as the final results. They are in good agreement with simulation, as plotted in Fig. 21: the four-stage oscillator shows about 6 dBc/Hz lower phase noise than the one-stage oscillator; the two-stage one shows the highest phase noise.

The FoMs are plotted in Fig. 22: the four-stage quadrature oscillator show about the same FoM as the single-stage *LC* oscillator over the whole frequency range; and the parallel-coupled two-stage one is 5–10 dB lower. The FoMs keep constant between 400 kHz and 1 MHz offset frequency, but drops gradually below 200 KHz. This is because the phase noise drops at -20 dBc/Hz per decade at large offset frequencies; but at small offset frequencies, it follows -30 dBc/Hz per decade [24]. Besides, the FoM of the four-stage LC-ring oscillator is slightly lower than the one-stage oscillator at offset frequencies above 400 kHz. This can be explained by the long metal traces between inductors, which have ohmic loss and introduce thermal noise. But at lower offset frequencies, where flicker noise from transistors dominates, the effect of this thermal noise is not significant any more and the two FoMs are exactly the same.

We measured the phase error with Agilent 54754A dual-channel TDR module. To compensate the possible asymmetry of probes and cables in the two signal paths, we switched the two pathes between the two quadrature outputs and measured the phase shift twice. Thus, the average values can rule out the asymmetry between the two signal pathes and

are listed in Table III. The four-stage LC-ring structure shows a phase error as low as $0.1°$, while the two-stage one is $1.9°$.

VIII. CONCLUSION

In this paper, we studied the dynamics and phase noise performance of distributed LC-ring oscillators. A mobius LC-ring oscillator with more than two stages can synthesize multiple phase while maintaining the high FoM as a single-stage *LC* oscillator, which was verified by simulation and measurement. This also provides a systematic way of trading power for phase noise.

ACKNOWLEDGMENT

REFERENCES

[1] S. L. J. Gierkink, S. Levantino, R. C. Frye, C. Samori, and V. Boccuzzi, "A low-phase-noise 5-GHz CMOS quadrature VCO using superharmonic coupling," *IEEE J. Solid-State Circuits*, vol. 38, pp. 1148–1154, Jul. 2003.

[2] J. Hauenschild, "A plastic packaged 10 Gb/s BiCMOS clock and data recovering 1:4-demultiplexer with external VCO," *IEEE J. Solid-State Circuits*, vol. 31, pp. 2056–2059, Dec. 1996.

[3] H. Noguchi, N. Yoshida, H. Uchida, M. Ozaki, S. Kanemitsu, and S. Wada, "A 40-Gb/s CDR circuit with adaptive decision-point control based on eye-opening monitor feedback," *IEEE J. Solid-State Circuits*, vol. 43, no. 12, pp. 2929–2938, Dec. 2008.

[4] S. Patnaik, N. Lanka, and R. Harjani, "A dual-mode architecture for a phased-array receiver based on injection locking in 0.13 μm CMOS," in *IEEE ISSCC Dig. Tech. Papers*, Feb. 2009, pp. 490–491.

[5] B. Razavi, "RF transmitter architectures and circuits," in *Proc. IEEE Custom Integrated Circuits Conf.*, 1999, pp. 197–204.

[6] H. Lee, O. Kim, G. Ahn, and D. Jeong, "A low-jitter 5000 ppm spread spectrum clock generator for multi-channel SATA transceiver in 0.18 um CMOS," in *IEEE ISSCC Dig. Tech. Papers*, 2005, pp. 162–163.

[7] T. H. Lee, *The Design of CMOS Radio-Requency Integrated Circuits*, 2nd ed. Cambridge, U.K.: Cambridge University Press, 2004.

[8] A. Rofougaran, J. Rael, M. Rofougaran, and A. Abidi, "A 900 MHz CMOS *LC* oscillator with quadrature outputs," in *IEEE ISSCC Dig. Tech. Papers*, Feb. 1996, pp. 392–393.

[9] J. J. Kim and B. Kim, "A low-phase-noise CMOS *LC* oscillator with a ring structure," in *IEEE ISSCC Dig. Tech. Papers*, Feb. 2000, pp. 430–431.

[10] J. van der Tang, P. van de Ven, D. Kasperkovitz, and A. van Roermund, "Analysis and design of an optimally coupled 5-GHz quadrature *LC* oscillator," *IEEE J. Solid-State Circuits*, vol. 37, no. 5, pp. 657–661, May 2002.

[11] X. Li, S. Shekhar, and D. J. Allstot, "Low-power gm-boosted LNA and VCO circuits in 0.18 μm CMOS," in *IEEE ISSCC Dig. Tech. Papers*, Feb. 2005, pp. 534–615.

[12] A. W. L. Ng and H. C. Luong, "A 1 V 17 GHz 5 mW quadrature CMOS VCO based on transformer coupling," in *IEEE ISSCC Dig. Tech. Papers*, Feb. 2006, pp. 711–720.

[13] I. R. Chamas and S. Raman, "Analysis and design of a CMOS phase-tunable injection-coupled *LC* quadrature VCO (PTIC-QVCO)," *IEEE J. Solid-State Circuits*, vol. 44, no. 3, pp. 784–796, Mar. 2009.

[14] P. Andreani and A. Fard, "A 2.3 GHz LC-tank CMOS VCO with optimal phase noise performance," in *IEEE ISSCC Dig. Tech. Papers*, Feb. 2006, pp. 691–700.

[15] A. Mazzanti and P. Andreani, "A 1.4 mW 4.90-to-5.65 GHz class-C CMOS VCO with an average FoM of 194.5 dBc/Hz," in *IEEE ISSCC Dig. Tech. Papers*, Feb. 2008, pp. 474–629.

[16] L. Roman, A. Bonfanti, S. Levantino, C. Samori, and A. L. Lacaita, "5-GHz oscillator array with reduced flicker up-conversion in 0.13-um CMOS," *IEEE J. Solid-State Circuits*, vol. 41, no. 11, pp. 2457–2467, Nov. 2006.

[17] G. V. Eleftheriades and K. G. Balmain, *Netative-Refraction Materials—Fundamental Principles and Applications*. Hoboken, NJ: Wiley, 2005.

[18] C. Caloz and T. Itoh, *Electromagnetic Metamaterials: Transmission Line Theory and Microwave Applications*. Hoboken, NJ: Wiley, 2006.

[19] H. Wu and A. Hajimiri, "Silicon-based distributed voltage controlled oscillators," *IEEE J. Solid-State Circuits*, vol. 36, no. 3, pp. 493–502, Mar. 2001.

[20] N. Tzartzanis and W. W. Walker, "A reversible poly-phase distributed VCO," in *IEEE ISSCC Dig. Tech. Papers*, Feb. 2006, pp. 2452–2461.

[21] J. Lee and B. Razavi, "A 40-Gb/s clock and data recovery circuit in 0.18 μm CMOS technology," *IEEE J. Solid-State Circuits*, vol. 38, no. 12, pp. 2181–2190, Dec. 2003.

[22] M. Z. Dooghabadi and S. Naseh, "Multi-phase signal generation using capacitive coupling of LC-VCOs," in *IEEE Int. Conf. Electronics, Circuits and Systems*, Dec. 2007, pp. 1087–1090.

[23] J. Park and M. P. Flynn, "Capacitively averaged multi-phase *LC* oscillators," in *IEEE Int. Symp. Circuits and Systems*, May 2005, vol. 3, pp. 2651–2654.

[24] A. Hajimiri and T. H. Lee, "A general theory of phase noise in electrical oscillators," *IEEE J. Solid-State Circuits*, vol. 33, no. 2, pp. 179–194, Feb. 1998.

[25] D. M. Pozar, *Microwave Engineering*, 3rd ed. New York: Wiley, 2005.

[26] P. Andreani and X. Wang, "On the phase-noise and phase-error performances of multiphase *LC* VCOs," *IEEE J. Solid-State Circuits*, vol. 39, no. 11, pp. 1883–1893, Nov. 2004.

[27] I. R. Chamas and S. Raman, "A comprehensive analysis of quadrature signal synthesis in cross-coupled RF VCOs," *IEEE Trans. Circuits Syst. I: Reg. Papers*, vol. 54, no. 4, pp. 689–703, Apr. 2007.

[28] A. Mirzaei, M. E. Heidari, R. Bagheri, S. Chehrazi, and A. A. Abidi, "The quadrature *LC* oscillator: A complete portrait based on injection locking," *IEEE J. Solid-State Circuits*, vol. 42, no. 9, pp. 1916–1932, Sep. 2007.

[29] J. J. Rael and A. A. Abidi, "Physical processes of phase noise in differential *LC* oscillators," in *Proc. IEEE Custom Integrated Circuits Conf. (CICC)*, May 2000, pp. 569–572.

[30] R. A. Horn and C. R. Johnson, *Matrix Analysis*. Cambridge, U.K.: Cambridge University Press, 1985.

[31] A. Hajimiri and T. H. Lee, "Design issues in CMOS differential *LC* oscillators," *IEEE J. Solid-State Circuits*, vol. 34, no. 5, pp. 717–724, May 1999.

[32] A. Demir, A. Mehrotra, and J. Roychowdhury, "Phase noise in oscillators: A unifying theory and numerical methods for characterization," *IEEE Trans. Circuits Syst. I: Fundam. Theory Applicat.*, vol. 47, no. 5, pp. 655–674, May 2000.

[33] A. Hajimiri, S. Limotyrakis, and T. H. Lee, "Jitter and phase noise in ring oscillators," *IEEE J. Solid-State Circuits*, vol. 34, no. 6, pp. 790–804, Jun. 1999.

[34] A. A. Abidi, "Phase noise and jitter in CMOS ring oscillators," *IEEE J. Solid-State Circuits*, vol. 41, no. 8, pp. 1803–1816, Aug. 2006.
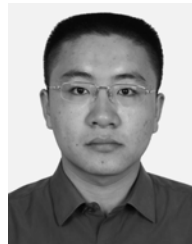
Guansheng Li received the B.Sc. and M.Sc. degrees in electronic engineering from Tsinghua University, Beijing, China, in 2005 and 2007, respectively. Since August 2007, he has been working toward the Ph.D. degree in electrical and computer engineering at Cornell University, Ithaca, NY.

His current research interest is mainly in radio-frequency integrated circuit design, with a focus on multi-phase and multi-band oscillator design and frequency synthesis. He also conducted research on wireless communications and networking, studying cross-layer optimization and wireless network coding.

Mr. Li serves as a reviewer for IEEE Transactions on Wireless Communications, IEEE Sensors Journal, and *Wireless Communications and Mobile Computing*. In 2007, he was named a Jacobs Scholar at Cornell University.

Ehsan Afshari (M'07) was born in 1979. He received the B.Sc. degree in electronics engineering from the Sharif University of Technology, Tehran, Iran, and the M.S. and Ph.D. degrees in electrical engineering from the California Institute of Technology, Pasadena, in 2003 and 2006, respectively.

In August 2006, he joined the faculty in Electrical and Computer Engineering at Cornell University, Ithaca, NY. His research interests are high-speed and low-noise integrated circuits for applications in communication systems, sensing, and biomedical devices.

Prof. Afshari serves as the chair of the IEEE Ithaca section, as the chair of Cornell Highly Integrated Physical Systems (CHIPS), and as a member of the Analog Signal Processing Technical Committee of the IEEE Circuits and Systems Society. He received the National Science Foundation CAREER Award in 2010, Cornell College of Engineering Michael Tien Excellence in Teaching Award in 2010, the Defense Advanced Research Projects Agency Young Faculty Award in 2008, and Iran's Best Engineering Student Award by the President of Iran in 2001. He is also the recipient of the Best Paper Award in the IEEE Custom Integrated Circuits Conference (CICC), September 2003, the First Place at the Stanford-Berkeley-Caltech Inventors Challenge, March 2005, the Best Undergraduate Paper Award in the Iranian Conference on Electrical Engineering 1999, the Silver Medal in the Physics Olympiad in 1997, and the Award of Excellence in Engineering Education from the Association of Professors and Scholars of Iranian Heritage (APSIH), May 2004.